

ManiTrend: Bridging Future Generation and Action Prediction with 3D Flow for Robotic Manipulation

Yuxin He Qiang Nie

The Hong Kong University of Science and Technology (Guangzhou)

21S051047@stu.hit.edu.cn

qiangnie@hkust-gz.edu.cn

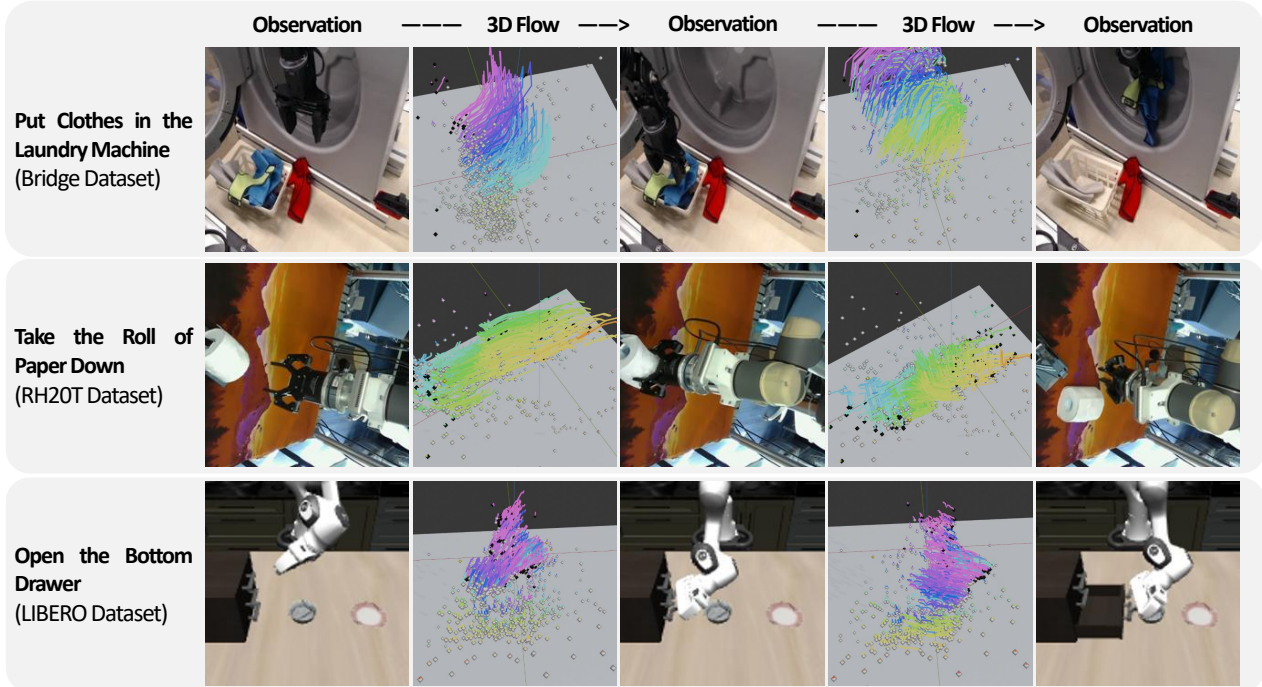


Fig. 1: Visualization of 3D flow, the future motion of particles within the 3D space, annotated with the SpatialTracker tool [44]. The trajectory of each sampled particle is colored, with its end point marked in black. We highlight the value of 3D flow as a bridge between pixel-wise spatial-temporal modeling and fine-grained action prediction.

Abstract—Language-conditioned manipulation is a vital but challenging robotic task due to the high-level abstraction of language. To address this, researchers have sought improved goal representations derived from natural language. In this paper, we highlight 3D flow - representing the motion trend of 3D particles within a scene - as an effective bridge between language-based future image generation and fine-grained action prediction. To this end, we develop ManiTrend, a unified framework that models the dynamics of 3D particles, vision observations and manipulation actions with a causal transformer. Within this framework, features for 3D flow prediction serve as additional conditions for future image generation and action prediction, alleviating the complexity of pixel-wise spatiotemporal modeling and providing seamless action guidance. Furthermore, 3D flow can substitute missing or heterogeneous action labels during large-scale pretraining on cross-embodiment demonstrations. Experiments on two comprehensive benchmarks demonstrate that our method achieves state-of-the-art performance with high efficiency. Our code and model checkpoints will be available upon acceptance.

I. INTRODUCTION

The ability to manipulate under language instruction is significant for a generalist robot. However, given the high-level abstract nature of language and the domain gap between language and vision, it is challenging to effectively condition visuomotor policy on language instruction [16].

Recently, many approaches have been introduced to address this challenge from different perspectives. Among them, five paradigms lead the trend, including: 1) text-image alignment pretraining [30, 26, 17, 31]; 2) future image generation pretraining [43, 48, 46, 12]; 3) leveraging large vision-language models (VLMs); 4) conditioning on generated goal images [4, 39, 21]; 5) conditioning on predicted flow [40, 42, 2, 45]. Despite the promising results they have achieved, each of them has its own drawback. Text-image alignment pretraining focuses on learning static semantic features while neglecting temporal features. Future image generation pretraining can deliver spatially and temporally aware representation but

enforces modeling all pixels, many of which are irrelevant to physical motion. Large VLMs and text-to-image models pretrained on Internet data excel at language understanding and can generate code/low-level actions for control or goal images for guidance, but all of them are slow to generate and infeasible for real-time interaction, where active distractors may exist [47] or the environment may change rapidly [49].

Flow-conditioning methods [1, 40, 42, 2, 45] avoid the above drawbacks by leveraging the future motion of a set of points predicted from language instruction and image observation to effectively and efficiently guide policy. However, existing studies all leave the flow prediction subtask to another standalone model, which prohibits its potential effect on enhancing representation learning. Besides, most of them use 2D flow within the image frame space, lacking the integrity of 3D motion.

In this work, we come up with **ManiTrend**, a novel framework that models the dynamics of 3D particles, vision observations and demonstrated actions with a single transformer. By pretraining on captioned videos and using 3D flow prediction as an auxiliary learning task, our model develops a motion-aware space-time representation space under lingual context. During imitation finetuning, 3D flow further bridges future image generation and fine-grained action prediction, leveraging its intermediate granularity. The integration of 3D flow alleviates the challenge of modeling pixel dynamics solely based on language, while also offering direct guidance for Cartesian end-effector actions in 3D space.

To label the motion of 3D particles on RGB videos, we leverage SpatialTracker [44] to track the position of densely-sampled grid points within a projected 3D space during data preprocessing. The labels of 3D flow (as illustrated in Figure 1) are then used to train our model to predict the future motion of a set of particles conditioned on language and observations. Features for 3D flow prediction also serve as additional condition for future image generation and action prediction, injected through various techniques such as self-attention and adaptive layer normalization.

To verify the proposed framework, we conduct pretraining across four real-world datasets and one simulated dataset with videos of human/robot manipulation, and carry out downstream experiments on two benchmark datasets (CALVIN [29], LIBERO [24]). Experimental results show that our method achieves high success rates that are competitive to or better than state-of-the-art (SoTA) while being more efficient.

Our contributions can be summarized as follows:

- We rediscover 3D flow as suitable a bridge between future generation and action prediction for robotic manipulation because of its intermediate granularity.
- We propose ManiTrend, a unified framework that tracks the dynamics of 3D particles, vision observations and manipulation actions with a single model.
- Experiments on two challenging benchmarks empirically show that our method achieves SoTA performance and is efficient by leveraging 3D flow. Our project will be fully open-source.

II. RELATED WORK

a) Language-conditioned manipulation: It is a natural way for humans to use language instructions to command robotic agents. Instead of constructing a single-task visuomotor policy for every possible instruction, it is more desirable to have a multitask language-conditioned manipulation policy that is generalizable and scalable. CLIPort [38], which injects frozen CLIP [35] language embeddings into two-stream convolution networks, is one of the first studies that show the potential of this paradigm. Some follow-up methods [3] adopt the same idea and replace the backbone with transformers. However, purely relying on frozen language embeddings will impose a limit of generalizability, due to the flexibility of language. In contrast, some methods employ large language models to generate code for manipulation [23, 14], which somehow solve the challenge of language conditioning, but are slow at inference and impractical for real-time closed-loop interaction, where active distractors may exist [47] or the environment itself may change rapidly [49]. This efficiency issue also hinders the application of methods that tune large vision-language models to generate action [5, 20], or leverage large diffusion models to translate instructions into goal images [4, 39, 21]. Compared to the above methods, representation learning approaches [30, 26, 17, 31, 43, 48, 46, 1] seem to be more promising, which incorporate auxiliary learning tasks to obtain language-aware features for manipulation. Our work adheres to this paradigm of representation learning.

b) Video pretraining for manipulation: Videos associated with language captions are much more accessible than robotic data while being suitable for learning language-aware spatial-temporal representations about manipulation behaviors. Some pioneering efforts leverage self-supervised learning tasks like time contrast [30, 27] and video-language alignment [16, 17]. More recent approaches prefer future image generation pretraining [43, 48, 46, 12], which delivers high-quality representations and good interpretability as a side product. However, it is essentially demanding. To generate a future frame based on history frames and a language caption, a model has to capture not only the movement and occlusion relations of objects but also their visual appearances [42]. In this work, we find it applicable to alleviate the burden of future image generation by providing guidance on movement and spatial relations through 3D flow.

c) Flow-enhanced manipulation policies: Different from modeling frame-to-frame transition, flow highlights a subset of points within the frame. As a result, movement information is decoupled from visual appearance information, becoming easier to get captured by a model. In [1], 2D flow prediction from the latent space of the policy model acts as an auxiliary learning task, while the predicted flow is not explicitly utilized for action guidance. In contrast, all other flow-enhanced manipulation policies [40, 42, 2, 45] solely employ predicted flow to guide action prediction. Among them, flow is typically confined into the 2D frame space and lacks the integrity of 3D physical motion, except for *General Flow* [45], which

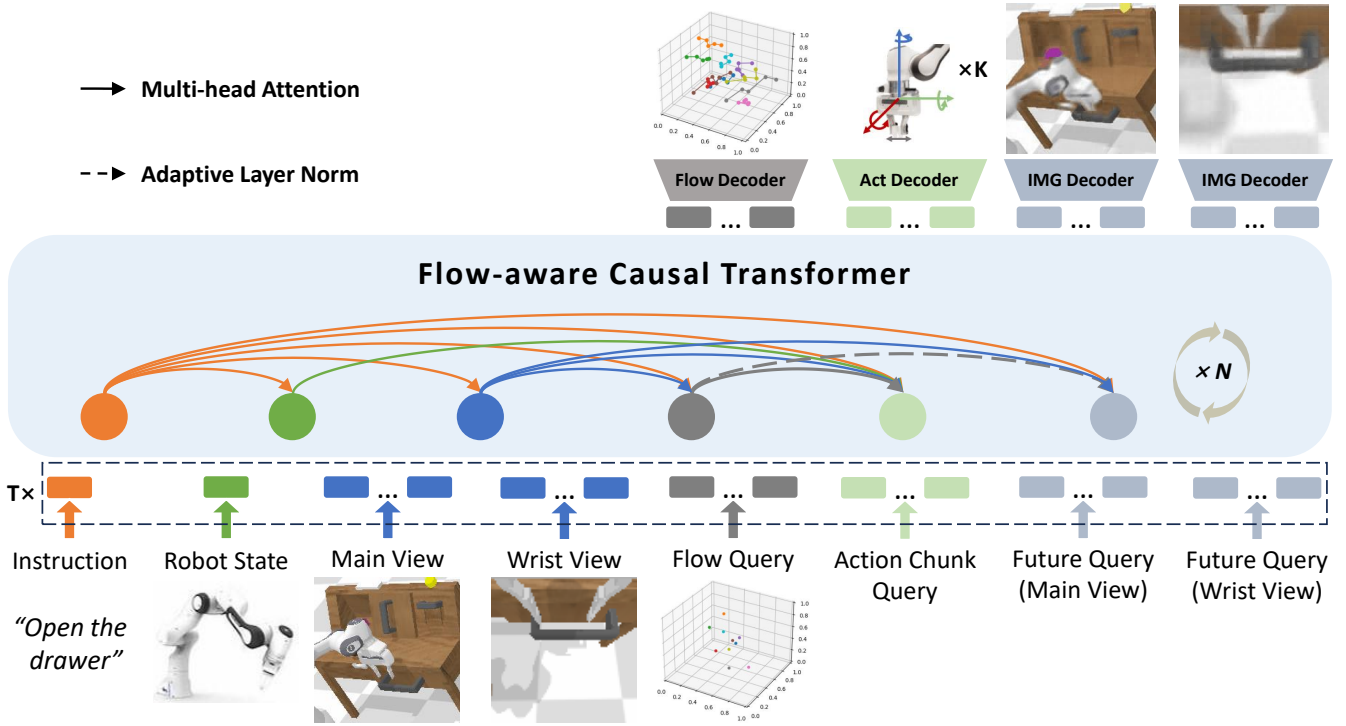


Fig. 2: An overview of ManiTrend, the proposed end-to-end framework that tracks the dynamics of 3D particles, vision observations and manipulation actions in a unified manner. Better viewed in color.

similarly adopts 3D flow as in this work. However, the main focus of *General Flow* [45] is to develop a 3D flow prediction model, whereas our work features the in-depth integration of 3D flow.

III. METHOD

A language-conditioned action-chunking policy $\pi_{\theta}(\mathbf{a}_{t:t+K-1} | \mathbf{o}_{t-T+1:t}, \mathbf{c})$ takes a language command \mathbf{c} and observations $\mathbf{o}_{t-T+1:t}$ (main/wrist-view images, robot proprioception states) with historical window size T as input, and outputs a chunk of actions $\mathbf{a}_{t:t+K-1}$ of length K . The three variables belong to quite distinct modalities, which is why auxiliary objectives that enhance representation learning are necessary. ManiTrend incorporates the prediction of 3D flow $\tau_{t:t+L-1} \in \mathbb{R}^{L \times P \times 3}$ and future images $\mathbf{i}_{t+S}^{\text{main/wrist}}$ in main/wrist views, where P is the number of track points, L is the flow length, S is the time shift of future images. In our formulation, the three dimensions of 3D flow correspond to x , y (in pixel coordinates), and absolute depth, respectively. The overall framework of our method is shown in Figure 2.

Following previous research [43, 21], the language command is encoded into a vector $\mathbf{c} \in \mathbb{R}^d$ (d is the model dimension) with CLIP [35] text encoder and a linear projection layer. Each main/wrist-view image is encoded into a matrix $\mathbb{I} \in \mathbb{R}^{(1+r) \times d}$ with MAE [13] and a perceiver resampler [15], where the first vector is the *CLS* token and the rest r vectors are resampled from the patch tokens. The robot proprioception state, which includes the 6D end-effector pose and the binary gripper status (closed or open), is embedded into a vector $\mathbf{p} \in \mathbb{R}^d$ with linear layers.

The construction of queries for flow, future images and action chunk is introduced below:

a) *Flow Query*: During training and inference, the model predicts the future 3D motion of grid points or randomly-sampled points that are near to grids. We initialize l learnable vectors $\mathbf{Q}^{\text{flow}} \in \mathbb{R}^{l \times d}$, as the embedding vectors of flow query. To include information about which points to track, the starting pixel coordinates of the sampled points are encoded into a vector via a linear layer, which is added to each flow query vector.

b) *Future Query*: Future query for main/wrist-view image is instantiated as $1 + r$ learnable vectors. The number of future query vectors is equal to the number of image embedding vectors, so appropriate capacity is equipped to reconstruct the representation of a future image.

c) *Action Chunk Query*: In GR-1 [43], a single vector is responsible for predicting a single-step action. To expand that for action chunking (predicting a sequence of actions [51]), we additionally initialize K learnable position embedding vectors. And a global learnable vector is added to each position embedding vector to form the final action chunk query.

A. Causal Dynamics Modeling with 3D Flow

The language/vision/proprioception input along with various queries for each timestep are organized into a sequence. And the sequences from timestep $t - T + 1$ to timestep t are concatenated and fed into a causal transformer. The causal transformer is essentially a transformer decoder, equipped with a carefully designed attention mask. Within it, all language/vision/proprioception tokens attend to their historical

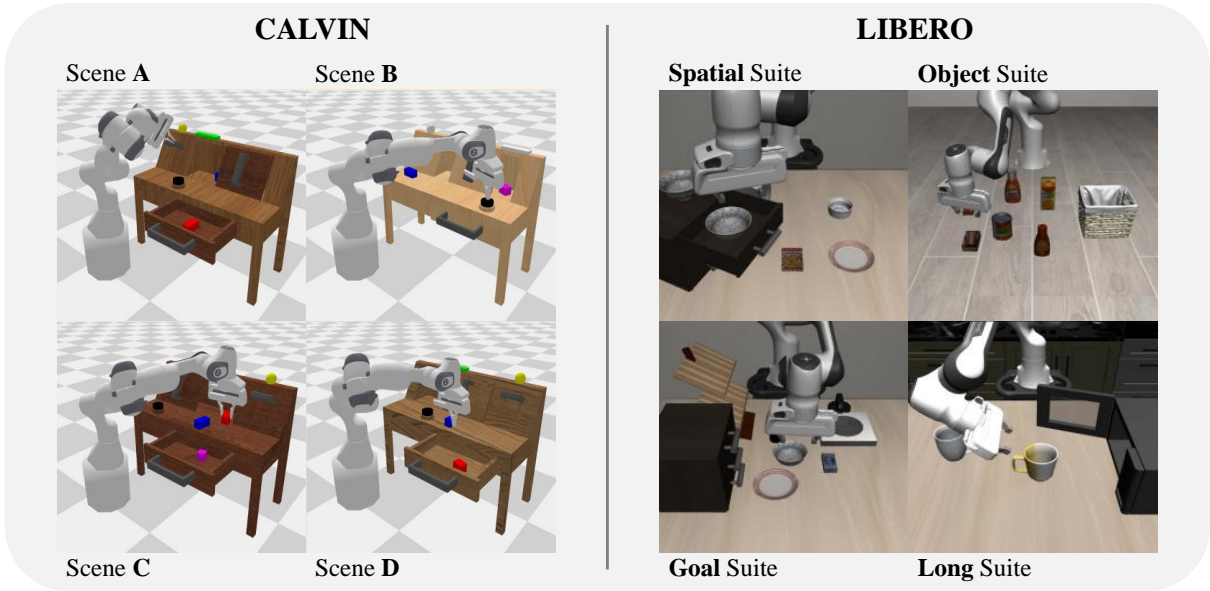


Fig. 3: Environments for our experiments. CALVIN involves 34 manipulation tasks and 4 scenes of different colors, textures and object placements. LIBERO features 4 evaluation task suites that challenge different dimensions of capability.

counterparts to establish temporal correlation. All queries attend to current and historical language/vision tokens, whereas action chunk queries additionally attend to current and historical proprioception tokens.

The interaction between various queries is centered on 3D flow, as detailed below.

1) *3D Flow for Future Image Generation*: Since the time shift S of the target future image is typically smaller than the flow length L (as it is harder to predict the future image than the future point position), we take a fraction of latent representation of flow query as an extra condition for future image generation. Concretely, within each transform block, the first $\lceil \frac{L(S+1)}{L} \rceil$ flow query vectors are pooled into a feature vector via 1D convolution. An MLP then turned the feature vector into gate, shift and scale vectors for the adaptive layer norm applied to future query before the Attention/MLP layer of the transform block. We employ adaptive layer norm [34] for conditioning because it is proven to be more effective than other approaches by recent research [33, 50].

2) *3D Flow for Action Chunk Prediction*: By default, we set the flow length L to be the same as the action chunk length K , since the two modalities are so similar in nature. And we enhance action prediction with the flow representation in a straightforward way, i.e., letting all action query vectors attend to all flow query vectors of the same timestep within each transform block.

B. Output Decoding

Queries are decoded into prediction of 3D flow, images and action chunk by downstream decoders, as described below.

1) *3D Flow Prediction*: The flow decoder resembles the track transformer proposed in [42], which first initiates a set of masked patch tokens from starting pixel coordinates, then updates patch representation conditioned on context and

linearly transforms the final patch representation into predicted flow $\hat{\tau}_{t:t+L-1} \in \mathbb{R}^{L \times P \times 3}$. The main difference is that the context used by [42] is the language/vision representation, whereas the context here is the final representation of flow query.

2) *Future Image Generation*: The image decoder works in a manner similar to the flow decoder, except that the input patch tokens are predefined as the sum of a learnable mask vector and 2D sin-cos positional embedding, which is a common practice in image reconstruction domain [9, 13].

3) *Action Chunk Prediction*: The K action query vectors are directly transformed into $\hat{\mathbf{a}}_{t:t+K-1}$, predicted actions corresponding to different current/future timesteps through an MLP layer. In this paper, we adopt the widely-used delta Cartesian action space, where an action includes translation (delta of x, y, z), rotation (delta of roll, pitch, yaw), and target binary closeness of the end-effector.

C. Learning Loss

The end-to-end learning loss \mathcal{L} over a data frame is the combination of 3D flow prediction loss $\mathcal{L}_{\text{flow}}$, future image generation \mathcal{L}_{img} and action chunk prediction loss \mathcal{L}_{act} , defined as follows:

$$\mathcal{L}_{\text{flow}} = \text{MSE}(\hat{\tau}_{t:t+L-1}, \tau_{t:t+L-1}) \quad (1)$$

$$\mathcal{L}_{\text{img}} = \text{MSE}(\hat{\mathbf{i}}_{t+S}^{\text{main}}, \mathbf{i}_{t+S}^{\text{main}}) + \text{MSE}(\hat{\mathbf{i}}_{t+S}^{\text{wrist}}, \mathbf{i}_{t+S}^{\text{wrist}}) \quad (2)$$

$$\mathcal{L}_{\text{act}} = \alpha \cdot \text{SmoothL1}(\hat{\mathbf{a}}_{t:t+K-1}[:6], \mathbf{a}_{t:t+K-1}[:6]) + \text{BCE}(\hat{\mathbf{a}}_{t:t+K-1}[6], \mathbf{a}_{t:t+K-1}[6]) \quad (3)$$

$$\mathcal{L} = \beta \cdot \mathcal{L}_{\text{flow}} + \mathcal{L}_{\text{img}} + \mathcal{L}_{\text{act}} \quad (4)$$

where MSE, SmoothL1 and BCE mean Mean Squared Error, Smooth L1 and Binary Cross Entropy respectively. By default, we empirically set $\alpha = 100$ and $\beta = 5$.

TABLE I: Overall performance of ManiTrend and baseline methods on the CALVIN benchmark under the in-domain setting (D→D, training and testing on scene D). During evaluation, 1000 chains of task instructions are randomly sampled, and the success rates of consecutive five tasks are recorded and averaged over the 1000 chains.

Method	No. Instructions in a Row (1000 Chains)					Avg. # Solved Tasks
	1	2	3	4	5	
HULC [28]	82.7%	64.9%	50.4%	38.5%	28.3%	2.64
RoboFlamingo [22]	86.0%	71.4%	58.5%	46.0%	34.9%	2.97
MDT [36]	93.7%	84.5%	74.1%	64.4%	55.6%	3.72
RoboUniView [25]	96.2%	88.8%	77.6%	66.6%	56.3%	3.85
ManiTrend (Ours)	<u>95.1%</u>	<u>86.3%</u>	<u>76.4%</u>	68.3%	60.6%	3.87

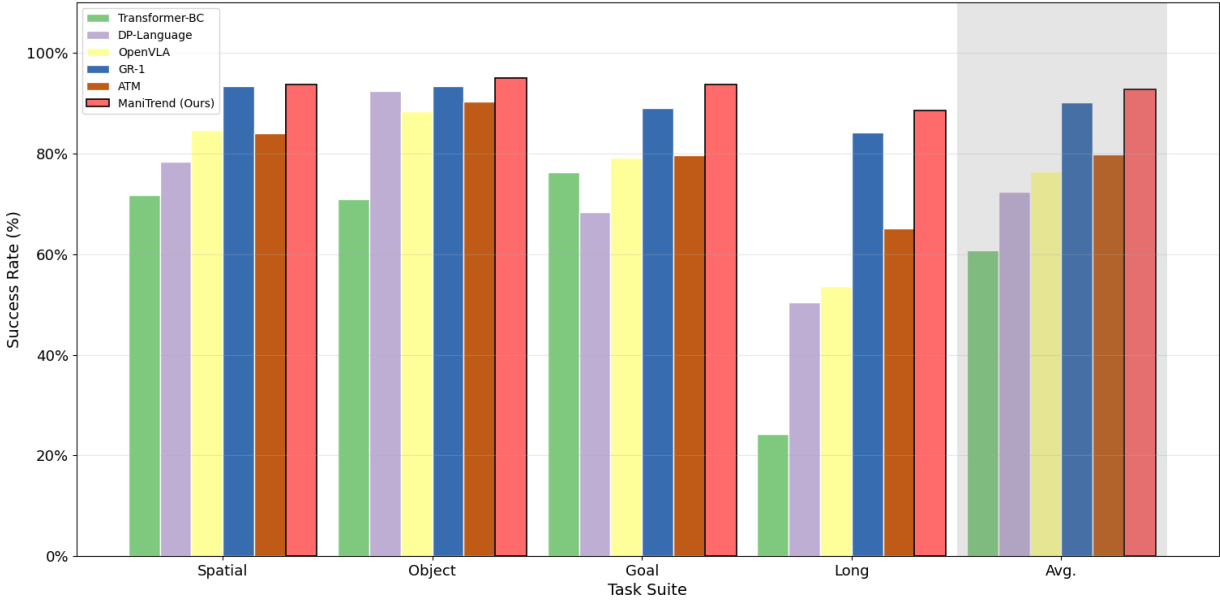


Fig. 4: Performance comparison on the 4 task suites of LIBERO benchmark. For each task suite, the success rate is calculated over 50 rollouts for each task within the task suite. The overall success rate is averaged over the results on the four task suites.

D. Cross-embodiment Pretraining

Our framework can be easily extended for large-scale pretraining on cross-embodiment manipulation demonstrations. Here, we do not bother to align the heterogeneous action labels, which is almost impossible because most datasets have different coordinates but do not provide relevant meta-data. Instead, we take advantage of 3D flow as an intermediary to learn the modes of physical motion within a scene. To avoid the negative impact of heterogeneous proprioception, we mask out the proprioception state tokens. Since wrist-view observation is unavailable in many datasets, we exclude wrist-view images from input and output during pretraining.

IV. EXPERIMENTS

Our experiments aim at addressing the following research questions:

- **Q1:** How is the performance of ManiTrend compared to SoTA language-conditioned manipulation policy models?
- **Q2:** Does modeling 3D flow help future generation?
- **Q3:** Does modeling 3D flow help action prediction?
- **Q4:** Is 3D flow superior to 2D flow?

- **Q5:** How much does cross-embodiment pretraining contribute to the performance of ManiTrend?

A. Implementation Details

When preprocessing training data with SpatialTracker [44], we employ a sampling strategy that results in around $\frac{1}{4}$ of the sampled points moving in the video and the others staying still. We do so in order to maintain a trade-off balance between teaching the model the motion of particles and narrowing the training-inference gap (since track points are just uniformly sampled from grids during inference).

We instantiate ManiTrend with 12 transformer blocks and model dimension of 384. The model weight is initialized with the GR-1 [43] checkpoint, which shares a similar architecture (except for the 3D flow related parts) and has been pretrained on Ego4D [11] videos. Our pretraining is then conducted on 44K trajectories from 5 datasets (RH20T [10], Bridge [41], Berkeley UR5 [7], Mutex [37] and LIBERO [24]) that cover 4 kinds of embodiments (humans, Franka robots, UR5 robots and WidowX robots). The pretraining process lasts for 35 epochs, which takes 3 days on 4 NVIDIA 4090 GPUs.

TABLE II: Comparison of zero-shot scene transfer ability on CALVIN (ABC→D, training on scenes A, B, C and testing on scene D).

Method	No. Instructions in a Row (1000 Chains)					Avg. # Solved Tasks
	1	2	3	4	5	
RoboFlamingo [22]	82.4%	61.9%	46.6%	33.1%	23.5%	2.47
GR-1 [43]	85.4%	71.2%	59.6%	49.7%	40.1%	3.06
3D Diffuser Actor [18]	92.2%	78.7%	63.9%	51.2%	41.2%	3.27
RoboUniView [25]	94.2%	84.2%	73.4%	62.2%	50.7%	3.64
GR-MG [21]	96.8%	89.3%	81.5%	72.7%	64.4%	4.04
ManiTrend (Ours)	95.0%	86.6%	77.9%	71.1%	63.0%	3.96

TABLE III: Comparison with SoTA language-conditioned manipulation policies in terms of inference speed. “T2I” stands for pretrained text-to-image models, e.g. Stable Diffusion.

Method	W. Large VLMs	W. Large T2I	Latency (ms)
OpenVLA [20]	✓		176
RoboUniView [25]	✓		105
GR-MG [21]		✓	121
ATM [42]			38
ManiTrend (Ours)			42

After that, we finetune and evaluate ManiTrend on downstream manipulation benchmarks CALVIN and LIBERO (Figure 3).

CALVIN [29] encompasses 34 manipulation tasks and 4 scenes (A, B, C, D) that are different in table colors, textures and object placements. The scenes along with a 7-DOF Franka robot are simulated via PyBullet. 5K expert trajectories (collected via teleoperation) with language instructions are provided for each scene. The benchmark features a challenging evaluation protocol: for each round, a chain of 5 task instructions is randomly sampled, and once the robot fails in one task, the following tasks are regarded as failed. Typically, there are 1000 rounds and the success flags of the consecutive five tasks are recorded for calculating the stage-wise success rates.

LIBERO [24] involves 130 tasks and 5 task suites (Spatial, Object, Goal, Long and 90). Each task suite has 10 tasks, except for the last task suite, which has 90 tasks. 50 (scripted) expert trajectories are provided for each task. Although the benchmark is originally designed for the life-long learning regime, it is also a good testbed for imitation learning algorithms. Following previous research [42, 20], we conduct finetuning and evaluation within each of the Spatial, Object, Goal, Long task suites.

B. In-domain Evaluation on CALVIN and LIBERO

For in-domain evaluation, language-conditioned multitask policies are trained with all expert data provided for a scene and tested on the same scene.

1) Baselines:

- **HULC** [28] is a hierarchical language-conditioned policy that leverages a global latent plan and representations refined with temporal visuo-lingual alignment.
- **RoboFlamingo** [22] utilizes VLMs for single-step vision language comprehension, and LSTM for modeling history information and predicting action.

- **RoboUniView** [25] enhances RoboFlamingo with a unified view representation, which is learned from the 3D occupancy task.
- **MDT** [36] is a transformer-based diffusion policy with the language representation aligned with the goal image representation.
- **GR-1** [43] is a GPT-style policy pretrained with text-to-video generation. It is originally tested on CALVIN and we additionally test it on LIBERO.
- **GR-MG** [21] enhances GR-1 with goal images generated by a finetuned InstructPix2Pix [6] model.
- **Transformer-BC** [24] is a vanilla language-conditioned transformer-based policy.
- **DP-Language** [8, 19] is a variant of diffusion policy, where language embedding is injected via concatenation.
- **OpenVLA** [20] directly extends large VLMs to predict discretized action by finetuning on OXE [32] data.
- **ATM** [42] incorporates 2D flow predicted by a track transformer to guide a transformer policy. We reproduce the results of it on LIBERO by training with full data.

2) *Results*: The results of comparison between ManiTrend and baselines under the in-domain setting (D→D, training and testing on scene D) of CALVIN are shown in Table I. It can be seen that ManiTrend surpasses SoTA methods MDT [36] and RoboUniView [25] by solving more consecutive tasks in average. The higher success rates on the last two tasks of a chain suggests that ManiTrend are more robust to unseen object placements and proprioception states (since the placement and state get more random as the rollout persists).

Figure 4 displays the in-domain evaluation results on the Spatial, Object, Goal and Long task suites of LIBERO. According to the results, ManiTrend consistently surpasses all baselines on the 4 task suites by a large margin. Interestingly, GR-1 [43] outperforms ATM [42], suggesting the guidance of 2D flow not necessarily works better than learning future image generation. And the superior performance of ManiTrend compared to GR-1 and ATM demonstrates the advantage of organically combining the two paradigms.

C. Zero-shot Scene Transfer on CALVIN

To evaluate the scene generalization capability of ManiTrend, we conduct zero-shot scene transfer experiments on CALVIN (ABC→D, training on scenes A, B, C and testing on scene D). The evaluation results are illustrated in Table II. We can see that ManiTrend outperforms most SoTA methods

TABLE IV: Results of Ablating 3D Flow for Future Generation.

3D Flow Prediction	3D Flow Conditioning	Pretrain (Validation)			CALVIN (D→D, Validation)		
		PSNR↑	SSIM↑	FID↓	PSNR↑	SSIM↑	FID↓
		22.80	0.6951	299.5	27.84	0.8608	110.3
✓		22.92	0.6966	295.7	27.95	0.8619	107.2
✓	✓	23.29	0.7011	289.2	28.29	0.8670	102.2

TABLE V: Results of Ablating 3D Flow for Action Prediction on CALVIN (D→D).

Dimension of Flow	Flow Prediction	Flow Conditioning	No. Instructions in a Row (1000 Chains)					Avg. # Solved Tasks
			1	2	3	4	5	
-			90.8%	81.1%	73.4%	67.4%	59.9%	3.80
3D	✓		93.3%	85.3%	76.6%	69.0%	61.0%	3.84
3D	✓	✓	95.1%	86.3%	76.4%	68.3%	60.6%	3.87
2D	✓	✓	94.0%	85.6%	76.3%	68.5%	60.6%	3.84

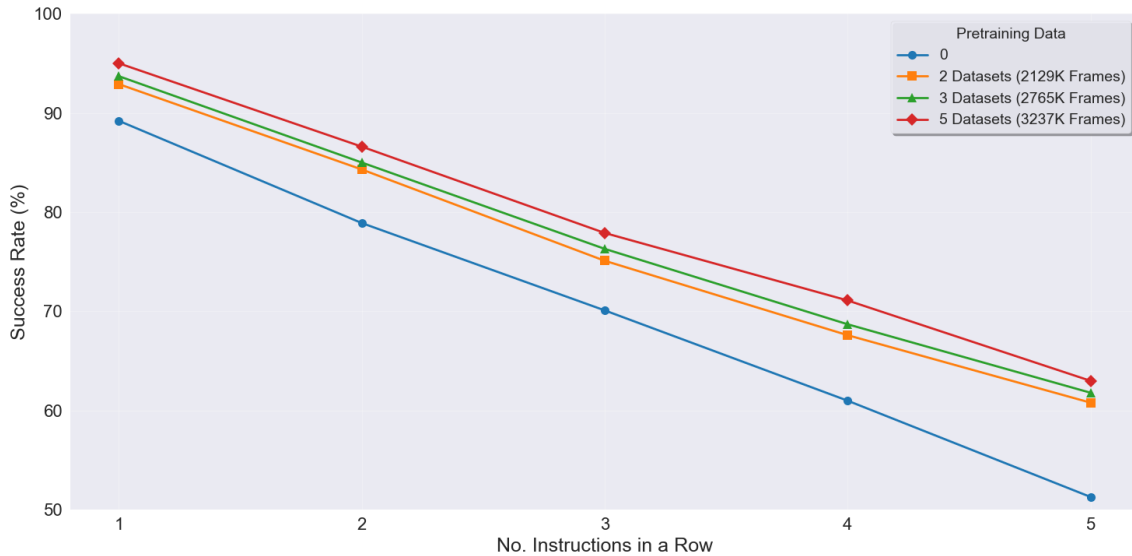


Fig. 5: Performance on CALVIN (ABC→D) of MainTrend pretrained with different amounts of data.

except for GR-MG, which takes advantage of the guidance of goal image generated by InstructPix2Pix [6], a large image editing diffusion model pretrained on high-quality Internet data. It is not surprising, as is known that Internet data breed the generalization ability of modern foundation models. And we believe that if pretraining ManiTrend with data of equal diversity and quality, ManiTrend will achieve similar level of generalization. Moreover, our method is much faster than GR-MG as analyzed in Section IV-D.

D. Inference Efficiency

In addition to the task success rate, inference efficiency is also an important dimension for evaluating a manipulation policy, which is always overlooked or concealed by recent research. If a policy is slow, it will not be able to react timely to a changing environment. Hence, a generalist manipulation policy should be a fast one. We compare the inference latencies of ManiTrend and SoTA language-conditioned manipulation policies running with a NVIDIA 4090 GPU. As shown in Table

III, methods that rely on large VLMs or text-to-image models to gain generalization ability, e.g. OpenVLA, RoboUniView and GR-MG tend to be quite slow, with latencies above 100 ms. Note that if we running these methods on an inferior on-board GPU instead of RTX 4090, the latencies will multiply, making it hard to even reach an operation frequency of 3 Hz. In contrast, methods that leverage flow for guidance, e.g. ManiTrend and ATM are able to operate about 3 times faster.

E. The Effect of 3D Flow on Future Generation

To verify the contribution of 3D flow to future generation, we compare the future image generation performance of ManiTrend with and without 3D flow prediction/conditioning. The results are illustrated in Table IV. After removing the adaptive layer norm module that conditions future generation on 3D flow feature, the measured quality of generated future images on both the validation sets of Pretrain data and CALVIN D→D data substantially degrades. Further removing the 3D flow prediction module leads to further degradation, but by a much

smaller margin. This indicates that simply learning to predict the 3D flow slightly contributes to learning future generation. Whereas injecting 3D flow feature into the future generation module does help a lot.

F. The Effect of 3D Flow on Action Prediction

We conduct ablation study on in-domain CALVIN evaluation setting (D→D) to look into the effect of 3D flow on action prediction. As shown in Table V, both 3D flow prediction and the attention from 3D flow query to action chunk query contribute to action prediction. Interestingly, adding the attention from 3D flow query substantially increases the success rates of first 2 tasks, but somehow hurts the performance on last few tasks, which means the model tends to overfit the object placements and proprioception states seen in training data. It is reasonable, considering the deep correlation between 3D flow and particles of objects/robots.

After replacing 3D flow with 2D flow, the task success rates decrease overall, demonstrating the superiority of 3D flow over 2D flow on guiding fine-grained control.

G. The Effect of Cross-embodiment Pretraining

To quantify the contribution of cross-embodiment pretraining to downstream performance, especially to generalization ability, we ablate the amount of pretraining data and measure the resulting performance on CALVIN (ABC→D). It can be observed from Figure 5 that: 1) When the amount of pretraining data goes from 0 to 2129K frames, the overall performance is greatly boosted, indicating the effectiveness of our pretraining. 2) The performance gain is more significant when adding 2 extra datasets than when adding 1 dataset with similar number of frames. This indicates that the diversity of pretraining data is more important than the quantity.

V. CONCLUSION AND DISCUSSION

In this paper, we introduce ManiTrend, an end-to-end framework for modeling the dynamics of 3D particles, vision observations and manipulation actions in a uniform manner. The design is motivated by the observation that 3D flow is a suitable intermediate for bridging future image generation and fine-grained action prediction, which is verified by our ablation study. As a flexible framework, ManiTrend supports cross-embodiment pretraining on manipulation demonstrations without using action labels. In-domain and zero-shot transfer evaluations on LIBERO and CALVIN demonstrate that ManiTrend achieves SoTA manipulation performance. In addition, it is much faster than SoTA methods that rely on large VLMs or text-to-image models. Experimental results also bring out two interesting discoveries: 1) letting action chunk query attend to flow query does help action prediction, but at the risk of overfitting the object placements and proprioception states seen in training data; 2) increasing the diversity of pretraining data is more helpful than increasing the quantity. Both facts indicate that diversity should be the primary consideration for scaling up pretraining/finetuning data. In the future, we will extend ManiTrend for bimanual manipulation and incorporate more sensory input, e.g. depth and force/torque.

VI. LIMITATIONS

We summarize the limitations of our work as follows:

- The quality of the 3D flow label highly depends on the tool we use, SpatialTracker [44], which is far from mature. It is likely that current performance of ManiTrend is restricted by this. But we believe that the fast-developing 3D Tracking technology will resolve this limitation.
- We have not investigated different model architectures, especially the structures of conditioning future generation and action prediction on 3D flow. A thorough empirical study on this may uncover better implementations that yield better performance.
- The 3D flow in this work only accounts for main view observation, and we have not looked into the influence of the length and density of flow.
- Some modalities of sensory input, e.g. depth, are not covered in this work, which may benefit 3D flow modeling.
- The manipulation tasks discussed in this work only involve a single arm.

REFERENCES

- [1] Homanga Bharadhwaj, Debidatta Dwivedi, Abhinav Gupta, Shubham Tulsiani, Carl Doersch, Ted Xiao, Dhruv Shah, Fei Xia, Dorsa Sadigh, and Sean Kirmani. Gen2act: Human video generation in novel scenarios enables generalizable robot manipulation. *arXiv preprint arXiv:2409.16283*, 2024.
- [2] Homanga Bharadhwaj, Roozbeh Mottaghi, Abhinav Gupta, and Shubham Tulsiani. Track2act: Predicting point tracks from internet videos enables diverse zero-shot robot manipulation. *arXiv preprint arXiv:2405.01527*, 2024.
- [3] Homanga Bharadhwaj, Jay Vakil, Mohit Sharma, Abhinav Gupta, Shubham Tulsiani, and Vikash Kumar. Roboagent: Generalization and efficiency in robot manipulation via semantic augmentations and action chunking. In *2024 IEEE International Conference on Robotics and Automation (ICRA)*, pages 4788–4795. IEEE, 2024.
- [4] Kevin Black, Mitsuhiko Nakamoto, Pranav Atreya, Homer Rich Walke, Chelsea Finn, Aviral Kumar, and Sergey Levine. Zero-shot robotic manipulation with pre-trained image-editing diffusion models. In *The Twelfth International Conference on Learning Representations*, 2024.
- [5] Anthony Brohan, Noah Brown, Justice Carbajal, Yevgen Chebotar, Xi Chen, Krzysztof Choromanski, Tianli Ding, Danny Driess, Avinava Dubey, Chelsea Finn, et al. Rt-2: Vision-language-action models transfer web knowledge to robotic control. *arXiv preprint arXiv:2307.15818*, 2023.
- [6] Tim Brooks, Aleksander Holynski, and Alexei A Efros. Instructpix2pix: Learning to follow image editing instructions. In *Proceedings of the IEEE/CVF Conference on Computer Vision and Pattern Recognition*, pages 18392–18402, 2023.

- [7] Lawrence Yunliang Chen, Simeon Adebola, and Ken Goldberg. Berkeley UR5 demonstration dataset. <https://sites.google.com/view/berkeley-ur5/home>, 2023.
- [8] Cheng Chi, Zhenjia Xu, Siyuan Feng, Eric Cousineau, Yilun Du, Benjamin Burchfiel, Russ Tedrake, and Shuran Song. Diffusion policy: Visuomotor policy learning via action diffusion. *The International Journal of Robotics Research*, page 02783649241273668, 2023.
- [9] Patrick Esser, Robin Rombach, and Bjorn Ommer. Taming transformers for high-resolution image synthesis. In *Proceedings of the IEEE/CVF conference on computer vision and pattern recognition*, pages 12873–12883, 2021.
- [10] Hao-Shu Fang, Hongjie Fang, Zhenyu Tang, Jirong Liu, Junbo Wang, Haoyi Zhu, and Cewu Lu. Rh20t: A robotic dataset for learning diverse skills in one-shot. In *RSS 2023 Workshop on Learning for Task and Motion Planning*, 2023.
- [11] Kristen Grauman, Andrew Westbury, Eugene Byrne, Zachary Chavis, Antonino Furnari, Rohit Girdhar, Jackson Hamburger, Hao Jiang, Miao Liu, Xingyu Liu, et al. Ego4d: Around the world in 3,000 hours of egocentric video. In *Proceedings of the IEEE/CVF Conference on Computer Vision and Pattern Recognition*, pages 18995–19012, 2022.
- [12] Haoran He, Chenjia Bai, Ling Pan, Weinan Zhang, Bin Zhao, and Xuelong Li. Large-scale actionless video pre-training via discrete diffusion for efficient policy learning. *arXiv preprint arXiv:2402.14407*, 2024.
- [13] Kaiming He, Xinlei Chen, Saining Xie, Yanghao Li, Piotr Dollár, and Ross Girshick. Masked autoencoders are scalable vision learners. In *Proceedings of the IEEE/CVF conference on computer vision and pattern recognition*, pages 16000–16009, 2022.
- [14] Siyuan Huang, Zhengkai Jiang, Hao Dong, Yu Qiao, Peng Gao, and Hongsheng Li. Instruct2act: Mapping multi-modality instructions to robotic actions with large language model. *arXiv preprint arXiv:2305.11176*, 2023.
- [15] Andrew Jaegle, Felix Gimeno, Andy Brock, Oriol Vinyals, Andrew Zisserman, and Joao Carreira. Perceiver: General perception with iterative attention. In *International conference on machine learning*, pages 4651–4664. PMLR, 2021.
- [16] Eric Jang, Alex Irpan, Mohi Khansari, Daniel Kappler, Frederik Ebert, Corey Lynch, Sergey Levine, and Chelsea Finn. Bc-z: Zero-shot task generalization with robotic imitation learning. In Aleksandra Faust, David Hsu, and Gerhard Neumann, editors, *Proceedings of the 5th Conference on Robot Learning*, volume 164 of *Proceedings of Machine Learning Research*, pages 991–1002. PMLR, 08–11 Nov 2022. URL <https://proceedings.mlr.press/v164/jang22a.html>.
- [17] Siddharth Karamcheti, Suraj Nair, Annie S. Chen, Thomas Kollar, Chelsea Finn, Dorsa Sadigh, and Percy Liang. Language-driven representation learning for robotics. In *Robotics: Science and Systems (RSS)*, 2023.
- [18] Tsung-Wei Ke, Nikolaos Gkanatsios, and Katerina Fragkiadaki. 3d diffuser actor: Policy diffusion with 3d scene representations. *arXiv preprint arXiv:2402.10885*, 2024.
- [19] Alexander Khazatsky, Karl Pertsch, Suraj Nair, Ashwin Balakrishna, Sudeep Dasari, Siddharth Karamcheti, Soroush Nasiriany, Mohan Kumar Srirama, Lawrence Yunliang Chen, Kirsty Ellis, et al. Droid: A large-scale in-the-wild robot manipulation dataset. *arXiv preprint arXiv:2403.12945*, 2024.
- [20] Moo Jin Kim, Karl Pertsch, Siddharth Karamcheti, Ted Xiao, Ashwin Balakrishna, Suraj Nair, Rafael Rafailov, Ethan Foster, Grace Lam, Pannag Sanketi, et al. Openvla: An open-source vision-language-action model. *arXiv preprint arXiv:2406.09246*, 2024.
- [21] Peiyan Li, Hongtao Wu, Yan Huang, Chilam Cheang, Liang Wang, and Tao Kong. Gr-mg: Leveraging partially annotated data via multi-modal goal conditioned policy. *arXiv preprint arXiv:2408.14368*, 2024.
- [22] Xinghang Li, Minghuan Liu, Hanbo Zhang, Cunjun Yu, Jie Xu, Hongtao Wu, Chilam Cheang, Ya Jing, Weinan Zhang, Huaping Liu, et al. Vision-language foundation models as effective robot imitators. *arXiv preprint arXiv:2311.01378*, 2023.
- [23] Jacky Liang, Wenlong Huang, Fei Xia, Peng Xu, Karol Hausman, Brian Ichter, Pete Florence, and Andy Zeng. Code as policies: Language model programs for embodied control. In *2023 IEEE International Conference on Robotics and Automation (ICRA)*, pages 9493–9500, 2023. doi: 10.1109/ICRA48891.2023.10160591.
- [24] Bo Liu, Yifeng Zhu, Chongkai Gao, Yihao Feng, Qiang Liu, Yuke Zhu, and Peter Stone. Libero: Benchmarking knowledge transfer for lifelong robot learning. *Advances in Neural Information Processing Systems*, 36, 2024.
- [25] Fanfan Liu, Feng Yan, Liming Zheng, Chengjian Feng, Yiyang Huang, and Lin Ma. Robouniview: Visual-language model with unified view representation for robotic manipulation. *arXiv preprint arXiv:2406.18977*, 2024.
- [26] Yecheng Jason Ma, Vikash Kumar, Amy Zhang, Osbert Bastani, and Dinesh Jayaraman. Liv: Language-image representations and rewards for robotic control. In *International Conference on Machine Learning*, pages 23301–23320. PMLR, 2023.
- [27] Yecheng Jason Ma, Shagun Sodhani, Dinesh Jayaraman, Osbert Bastani, Vikash Kumar, and Amy Zhang. Vip: Towards universal visual reward and representation via value-implicit pre-training. In *The Eleventh International Conference on Learning Representations*, 2023.
- [28] Oier Mees, Lukas Hermann, and Wolfram Burgard. What matters in language conditioned robotic imitation learning over unstructured data. *IEEE Robotics and Automation Letters*, 7(4):11205–11212, 2022.
- [29] Oier Mees, Lukas Hermann, Erick Rosete-Beas, and Wolfram Burgard. Calvin: A benchmark for language-conditioned policy learning for long-horizon robot ma-

- manipulation tasks. *IEEE Robotics and Automation Letters (RA-L)*, 7(3):7327–7334, 2022.
- [30] Suraj Nair, Aravind Rajeswaran, Vikash Kumar, Chelsea Finn, and Abhinav Gupta. R3m: A universal visual representation for robot manipulation. In *Conference on Robot Learning*, pages 892–909. PMLR, 2023.
- [31] Nghia Nguyen, Minh Nhat Vu, Tung D Ta, Baoru Huang, Thieu Vo, Ngan Le, and Anh Nguyen. Robotic-clip: Fine-tuning clip on action data for robotic applications. *arXiv preprint arXiv:2409.17727*, 2024.
- [32] Abby O’Neill, Abdul Rehman, Abhinav Gupta, Abhiram Maddukuri, Abhishek Gupta, Abhishek Padalkar, Abraham Lee, Acorn Pooley, Agrim Gupta, Ajay Mandlikar, et al. Open x-embodiment: Robotic learning datasets and rt-x models. *arXiv preprint arXiv:2310.08864*, 2023.
- [33] William Peebles and Saining Xie. Scalable diffusion models with transformers. In *Proceedings of the IEEE/CVF International Conference on Computer Vision*, pages 4195–4205, 2023.
- [34] Ethan Perez, Florian Strub, Harm De Vries, Vincent Dumoulin, and Aaron Courville. Film: Visual reasoning with a general conditioning layer. In *Proceedings of the AAAI conference on artificial intelligence*, volume 32, 2018.
- [35] Alec Radford, Jong Wook Kim, Chris Hallacy, Aditya Ramesh, Gabriel Goh, Sandhini Agarwal, Girish Sastry, Amanda Askell, Pamela Mishkin, Jack Clark, et al. Learning transferable visual models from natural language supervision. In *International conference on machine learning*, pages 8748–8763. PMLR, 2021.
- [36] Moritz Reuss, Ömer Erdiñç Yağmurlu, Fabian Wenzel, and Rudolf Lioutikov. Multimodal diffusion transformer: Learning versatile behavior from multimodal goals. In *First Workshop on Vision-Language Models for Navigation and Manipulation at ICRA 2024*, 2024.
- [37] Rutav Shah, Roberto Martín-Martín, and Yuke Zhu. Mutex: Learning unified policies from multimodal task specifications. *arXiv preprint arXiv:2309.14320*, 2023.
- [38] Mohit Shridhar, Lucas Manuelli, and Dieter Fox. Cliport: What and where pathways for robotic manipulation. In *Conference on robot learning*, pages 894–906. PMLR, 2022.
- [39] Mohit Shridhar, Yat Long Lo, and Stephen James. Generative image as action models. In *8th Annual Conference on Robot Learning*, 2024.
- [40] Mel Vecerik, Carl Doersch, Yi Yang, Todor Davchev, Yusuf Aytar, Guangyao Zhou, Raia Hadsell, Lourdes Agapito, and Jon Scholz. Robotap: Tracking arbitrary points for few-shot visual imitation. In *2024 IEEE International Conference on Robotics and Automation (ICRA)*, pages 5397–5403. IEEE, 2024.
- [41] Homer Rich Walke, Kevin Black, Tony Z Zhao, Quan Vuong, Chongyi Zheng, Philippe Hansen-Estruch, Andre Wang He, Vivek Myers, Moo Jin Kim, Max Du, et al. Bridgedata v2: A dataset for robot learning at scale. In *Conference on Robot Learning*, pages 1723–1736. PMLR, 2023.
- [42] Chuan Wen, Xingyu Lin, John So, Kai Chen, Qi Dou, Yang Gao, and Pieter Abbeel. Any-point trajectory modeling for policy learning. *arXiv preprint arXiv:2401.00025*, 2023.
- [43] Hongtao Wu, Ya Jing, Chilam Cheang, Guangzeng Chen, Jiafeng Xu, Xinghang Li, Minghuan Liu, Hang Li, and Tao Kong. Unleashing large-scale video generative pre-training for visual robot manipulation. In *The Twelfth International Conference on Learning Representations*, 2024.
- [44] Yuxi Xiao, Qianqian Wang, Shangzhan Zhang, Nan Xue, Sida Peng, Yujun Shen, and Xiaowei Zhou. Spatial-tracker: Tracking any 2d pixels in 3d space. In *Proceedings of the IEEE/CVF Conference on Computer Vision and Pattern Recognition (CVPR)*, 2024.
- [45] Mengda Xu, Zhenjia Xu, Yinghao Xu, Cheng Chi, Gordon Wetzstein, Manuela Veloso, and Shuran Song. Flow as the cross-domain manipulation interface. In *8th Annual Conference on Robot Learning*, 2024.
- [46] Jiange Yang, Bei Liu, Jianlong Fu, Bocheng Pan, Gangshan Wu, and Limin Wang. Spatiotemporal predictive pre-training for robotic motor control. *arXiv preprint arXiv:2403.05304*, 2024.
- [47] Jichuan Yu, Zhao Jin, Chuxiong Hu, Jizhou Yan, Ze Wang, and Yu Zhu. Hierarchical real-time motion planning for safe multi-robot manipulation in dynamic environments. In *2024 International Conference on Advanced Robotics and Mechatronics (ICARM)*, pages 113–119. IEEE, 2024.
- [48] Jia Zeng, Qingwen Bu, Bangjun Wang, Wenke Xia, Li Chen, Hao Dong, Haoming Song, Dong Wang, Di Hu, Ping Luo, et al. Learning manipulation by predicting interaction. *arXiv preprint arXiv:2406.00439*, 2024.
- [49] Yuanhang Zhang, Tianhai Liang, Zhenyang Chen, Yanjie Ze, and Huazhe Xu. Catch it! learning to catch in flight with mobile dexterous hands. *arXiv preprint arXiv:2409.10319*, 2024.
- [50] Zhenghao Zhang, Junchao Liao, Menghao Li, Zuozhuo Dai, Bingxue Qiu, Siyu Zhu, Long Qin, and Weizhi Wang. Tora: Trajectory-oriented diffusion transformer for video generation. *arXiv preprint arXiv:2407.21705*, 2024.
- [51] Tony Z Zhao, Vikash Kumar, Sergey Levine, and Chelsea Finn. Learning fine-grained bimanual manipulation with low-cost hardware. *arXiv preprint arXiv:2304.13705*, 2023.

APPENDIX A PRETRAINING DATA

Data for pretraining includes 44K trajectories from 5 datasets (RH20T [10], Bridge [41], Berkeley UR5 [7], Mutex [37] and LIBERO [24]), which cover 4 kinds of embodiments (humans, Franka robots, UR5 robots and WidowX robots). For RH20T, we only use the data in configs 4 and 5. For Bridge, we filter out data without wrist-view observation (although

TABLE VI: Statistics of datasets used in our pretraining.

Dataset	Subset?	Embodiment	# Tasks	# Traj.	# Frames	Avg. Len.
RH20T [10]	Cfg 4, Cfg 5	Human, UR5, Franka	149	18264	1625166	89
Bridge [41]	Filtered	WidowX	13	18373	615772	34
LIBERO [24]	LIBERO-90	Franka	90	4500	673386	150
Berkeley UR5 [7]	Full Data	UR5	5	1000	96939	97
Mutex [37]	Full Data	Franka	100	1380	157095	114

TABLE VII: Hyperparameter settings

Hyperparameter	Pretraining	Finetuning (CALVIN)	Finetuning (LIBERO)
Epochs	35	40	50
Warmup epochs	2	1	1
Batchsize	960	560	288
Learning rate	5e-4	1e-3	5e-4
Gradient clip	0.1	-	-
Augment prob.	0.9	0.9	0.9
History window T	10	10	10
Time shift S	3	3	3
Flow length L	7	7	7
# track point P	50	50	50
Action chunk size K	7	7	7
# resampled vectors r	9	9	9
# flow query vectors l	4	4	4

we do not utilize wrist-view observation during pretraining, we filter the data for upward compatibility). For LIBERO, we use the data in LIBERO-90 task suite. It may be beneficial to add data from the other 4 task suites of LIBERO, but we leave it for future work. Detailed statistics of the pretraining data are listed in Table VI.

APPENDIX B NETWORK AND TRAINING DETAILS

There are about 200M parameters in ManiTrend. The backbone of ManiTrend is a causal transformer with 12 layers, 12 attention heads, a dropout rate of 0.1 and a latent size of 384. The number of resampled image feature vectors r and the number of flow query vectors l are set to 9 and 4 respectively. Both the flow decoder and future image decoder are made up of self-attention blocks and MLP layers. The action decoder is a three-layer MLP, where the last layer splits into two heads for predicting end-effector Cartesian actions and binary gripper closeness actions.

By default, we set historical window size T as 10, future time shift S as 3, flow length L as 7, the number of track points P as 50, and action chunk size K as 7 (only applicable to finetuning). Throughout pretraining and finetuning, images are augmented with random shift. The pretraining process lasts for 35 epochs, which takes about 3 days on 4 RTX 4090 GPUs. The finetuning process on CALVIN lasts for 40 epochs, taking around 0.5 day / 1.5 day on 4 RTX 4090 for D→D / ABC→D. The finetuning process on each task suite of LIBERO lasts for 50 epochs, taking about 10 hours on 2 RTX 4090. We employ the AdamW optimizer together with the cosine warmup strategy. Detailed hyperparameter settings are available in Table VII.

APPENDIX C

QUALITATIVE ANALYSIS OF PREDICTED 3D FLOW

We look into the 3D flow prediction performance on CALVIN and LIBERO. Qualitative results are shown in Figure 6 and Figure 7. It can be observed that:

- The quality of predicted 3D flow is overall satisfying, demonstrating the effectiveness of learning to model 3D flow.
- ManiTrend is good at modeling the flow of particles on the robotic arm, but weak at distinguishing between particles nearby the robotic arm and particles on the robotic arm.
- The density of moving particles that get sampled is relatively small. It is unclear whether increasing the density of tracking points will improve performance or not.
- 3D flow conveys valuable depth information, which is useful for tasks that involve rotation and longitudinal movement. In contrast, 2D flow misses depth information in certain direction.

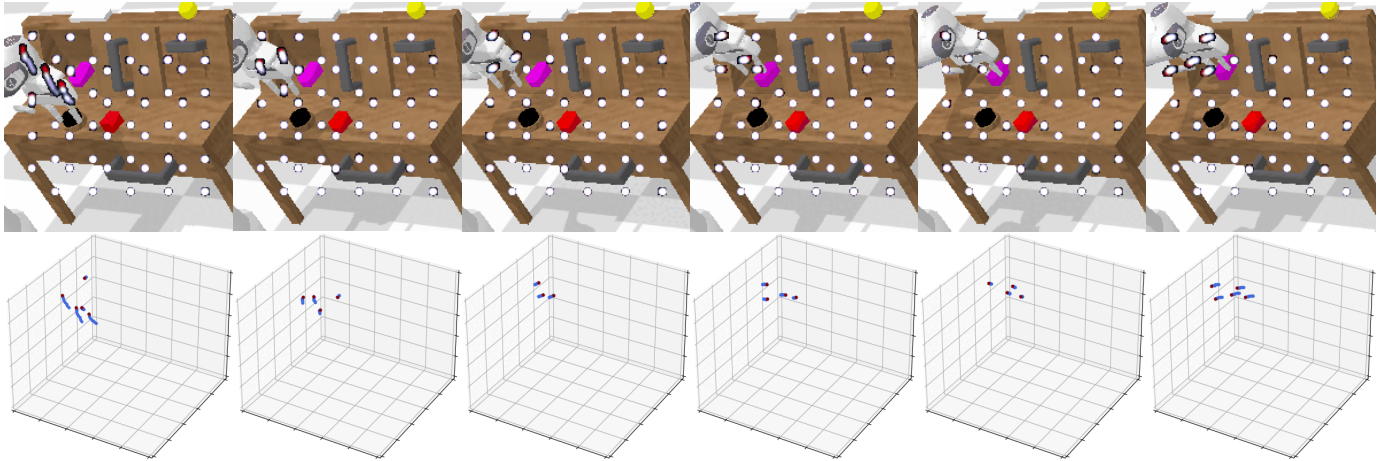
APPENDIX D

QUALITATIVE ANALYSIS OF GENERATED FUTURE IMAGES

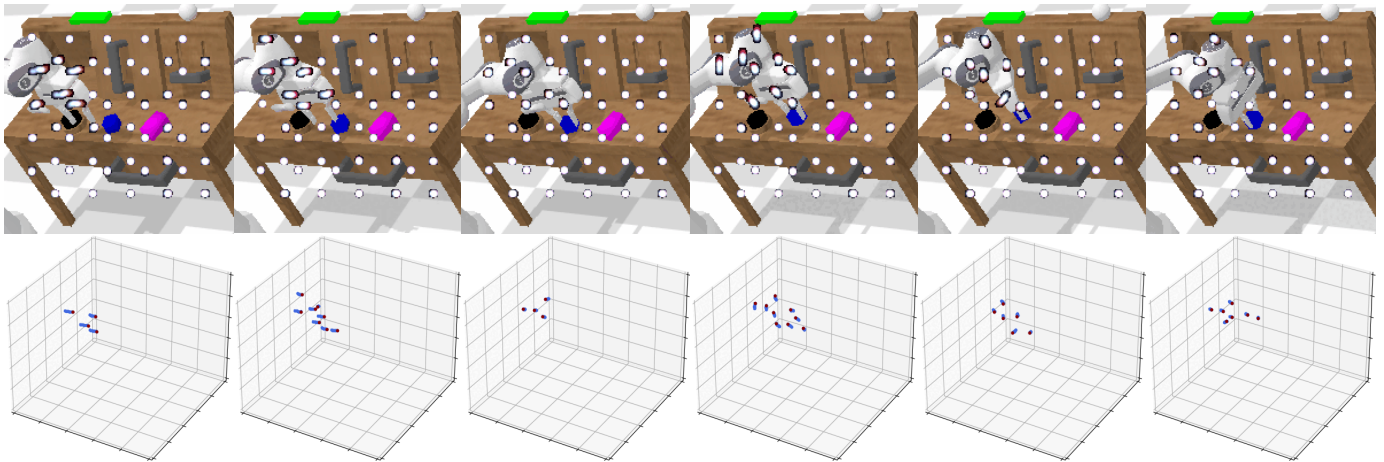
Figures 8 and 9 display the future images generated during rollouts on CALVIN and LIBERO. It can be observed that:

- The overall quality of the generated future images is satisfying, showcasing the effectiveness of spatiotemporal modeling.
- The distortion of the shapes and colors of objects is noticeable. And some images exhibit rasterization artifacts. These are caused by the suboptimal design of our image decoder. Using a stronger image decoder (such as the one in VQGAN [9]) may help address the problem.

Task: Lift the pink block



Task: Rotate the blue block right



Task: Place in the slider

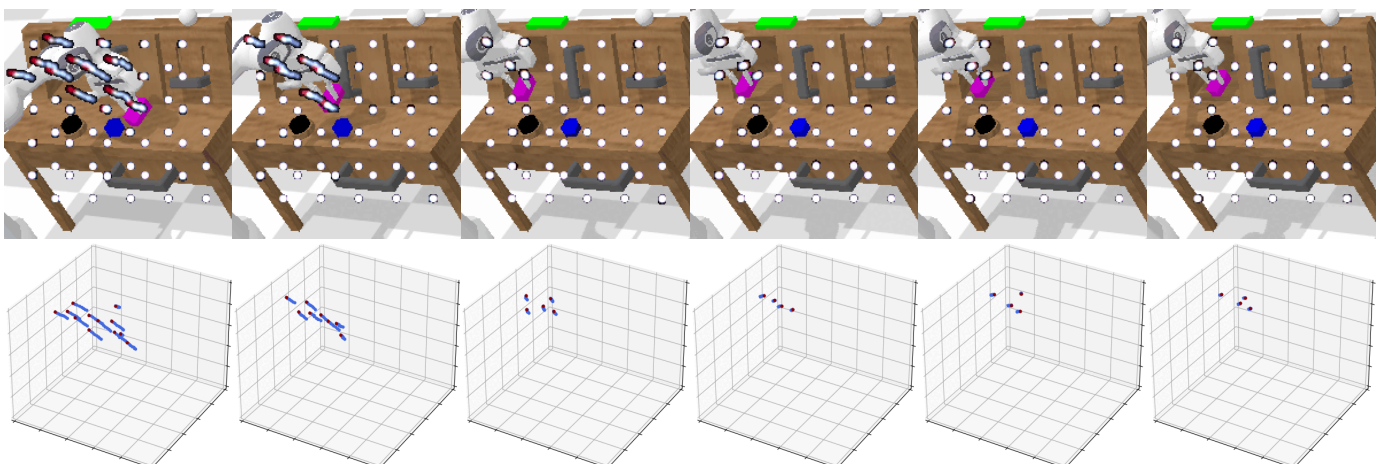
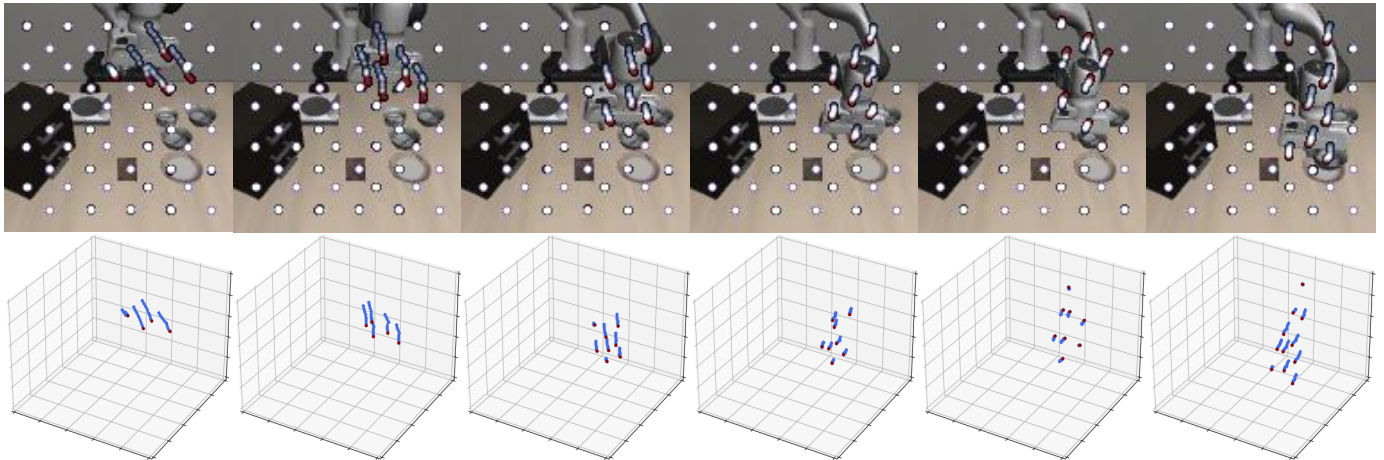
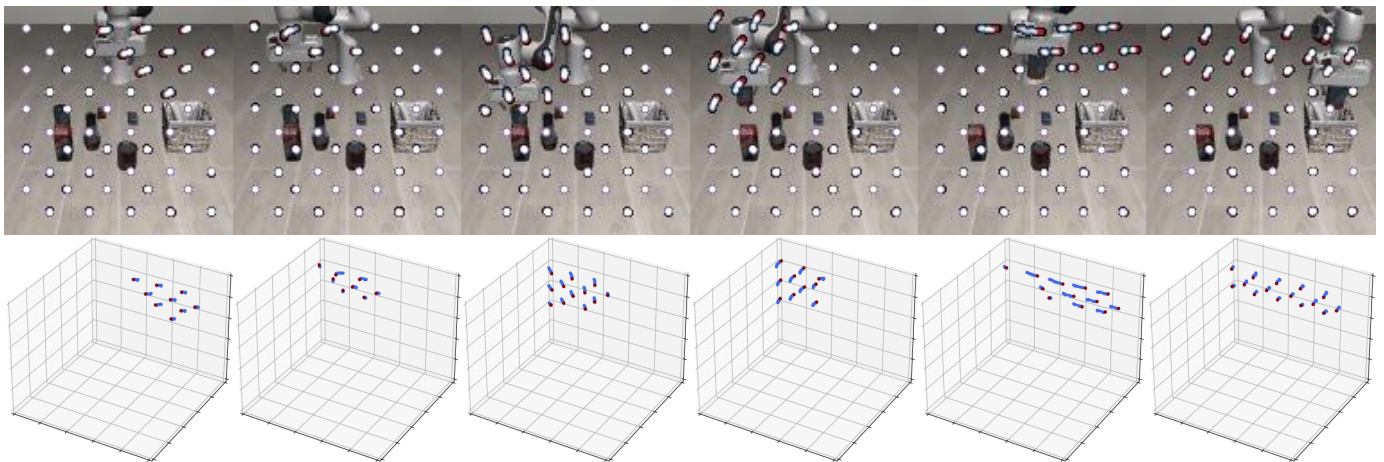


Fig. 6: Visualization of predicted 3D flow on CALVIN (D→D). The images in the upper row are main-view observations with rendered flow (only x, y are considered). Whereas the images in lower row visualize 3D flow in 3D space (for visual clarity, we only visualize the flow of moving particles that get sampled).

(Spatial) Task: Pick up the black bowl between the plate and the ramekin and place it on the plate



(Object) Task: Pick up the alphabet soup and place it in the basket



(Goal) Task: Open the middle drawer of the cabinet

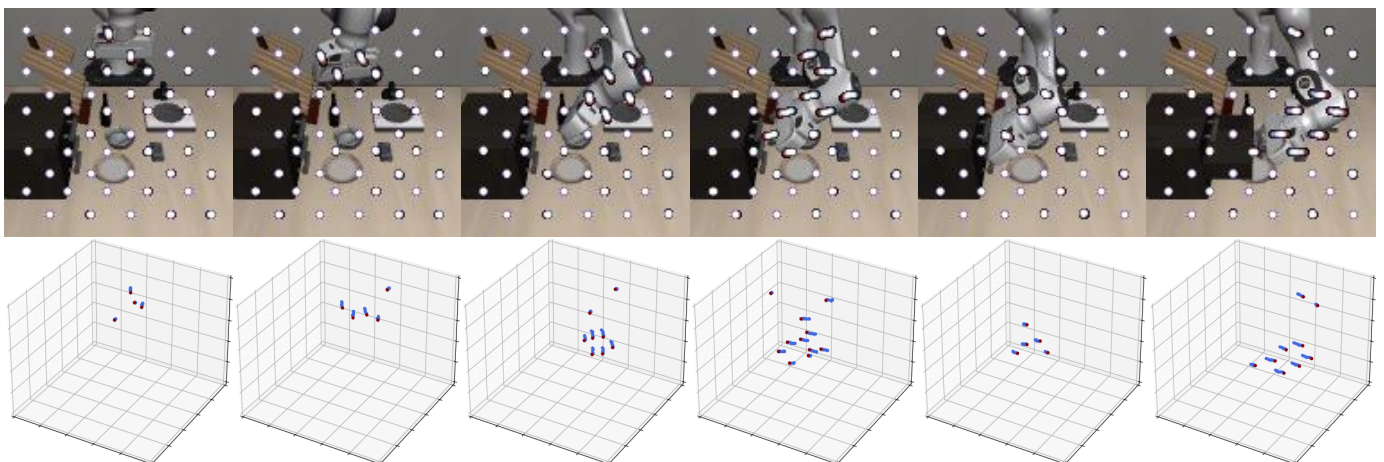
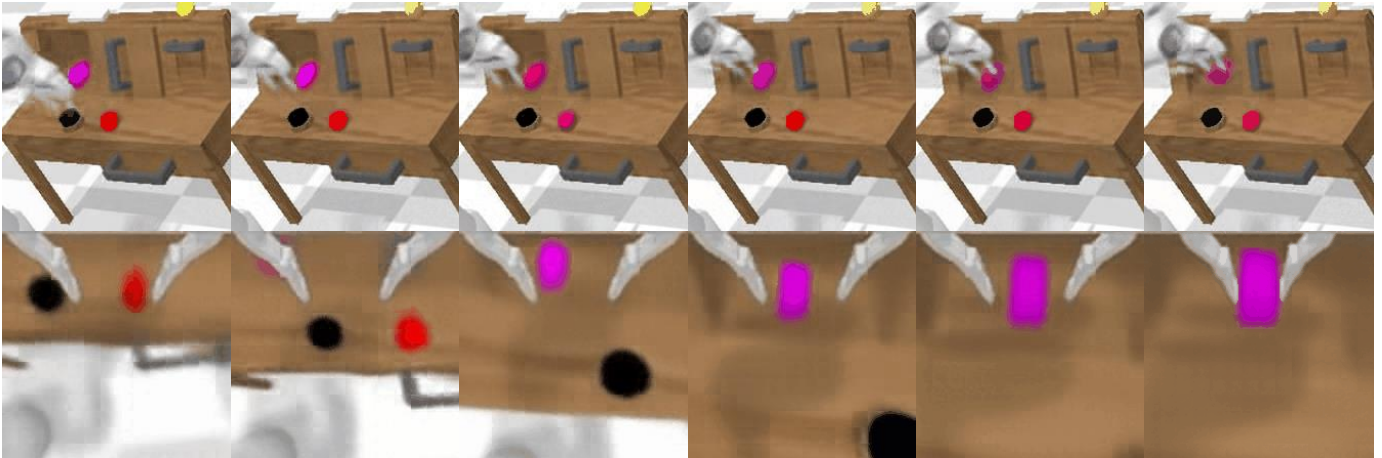
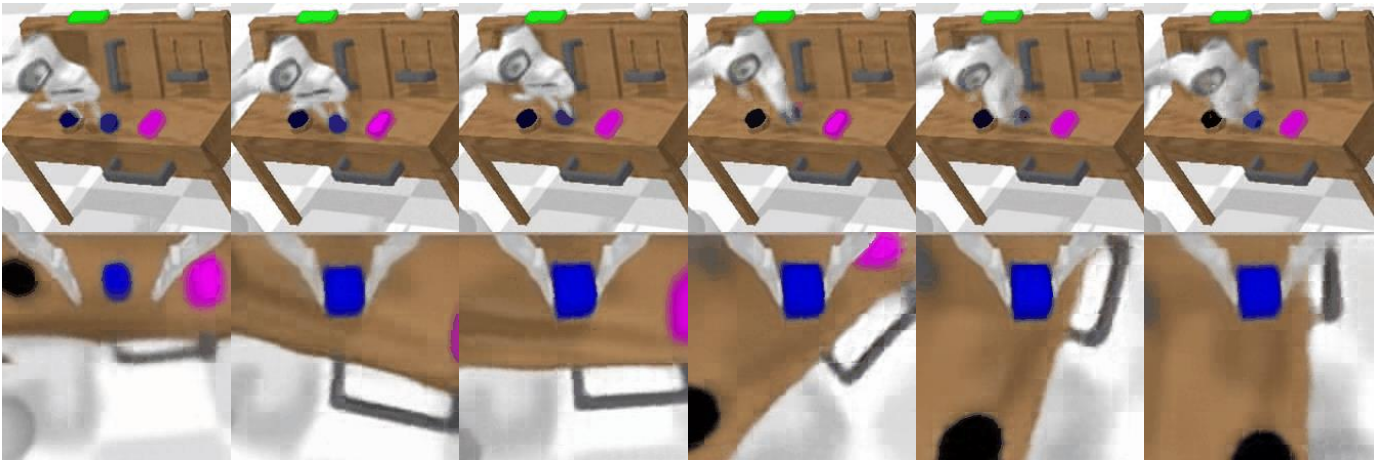


Fig. 7: Visualization of predicted 3D flow on the Spatial, Object and Goal task suites of LIBERO.

Task: Lift the pink block



Task: Rotate the blue block right



Task: Place in the slider

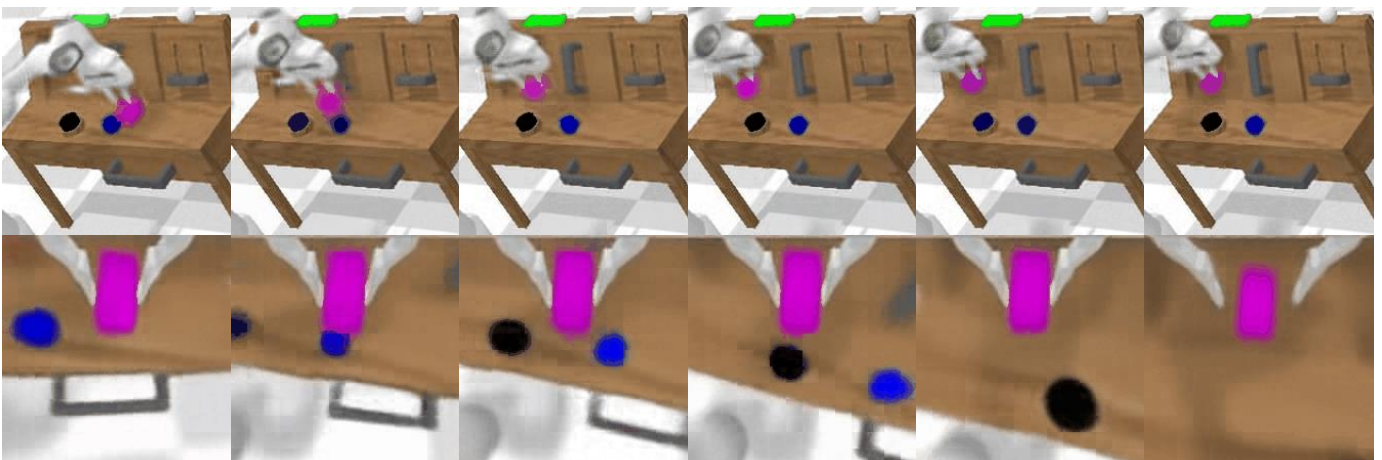
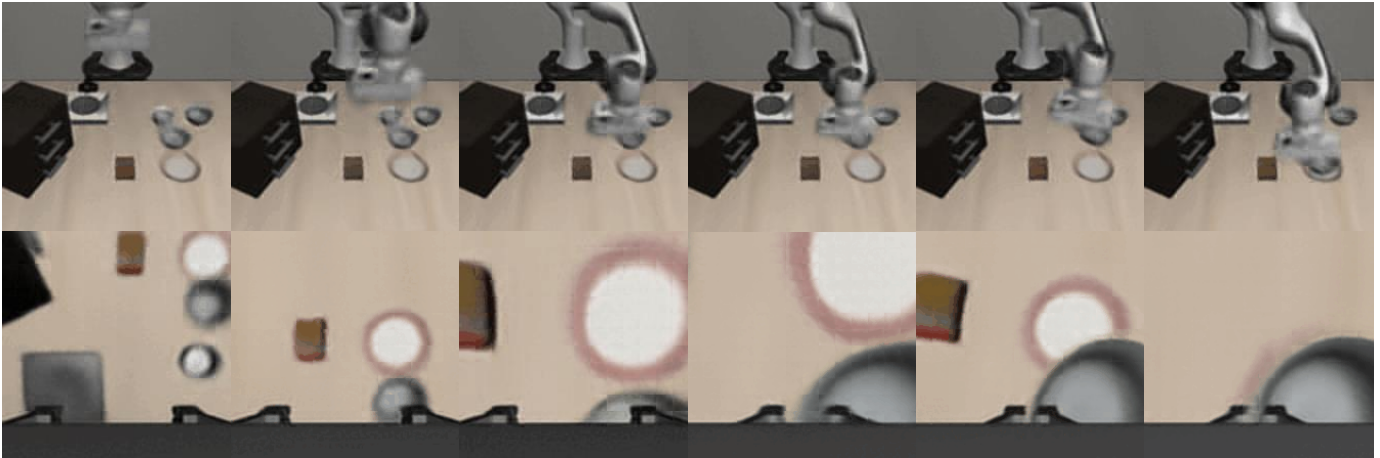


Fig. 8: Generated future main-view and wrist-view images on CALVIN (D→D).

(Spatial) Task: Pick up the black bowl between the plate and the ramekin and place it on the plate



(Object) Task: Pick up the alphabet soup and place it in the basket



(Goal) Task: Open the middle drawer of the cabinet



Fig. 9: Generated future main-view and wrist-view images on the Spatial, Object and Goal task suites of LIBERO.